

# LEGO-Net: Learning Regular Rearrangements of Objects in Rooms

QiuHong Anna Wei<sup>1</sup>   Sijie Ding<sup>\*1</sup>   Jeong Joon Park<sup>\*2</sup>   Rahul Sajnani<sup>1</sup>  
 Adrien Poulenard<sup>2</sup>   Srinath Sridhar<sup>1</sup>   Leonidas Guibas<sup>2</sup>

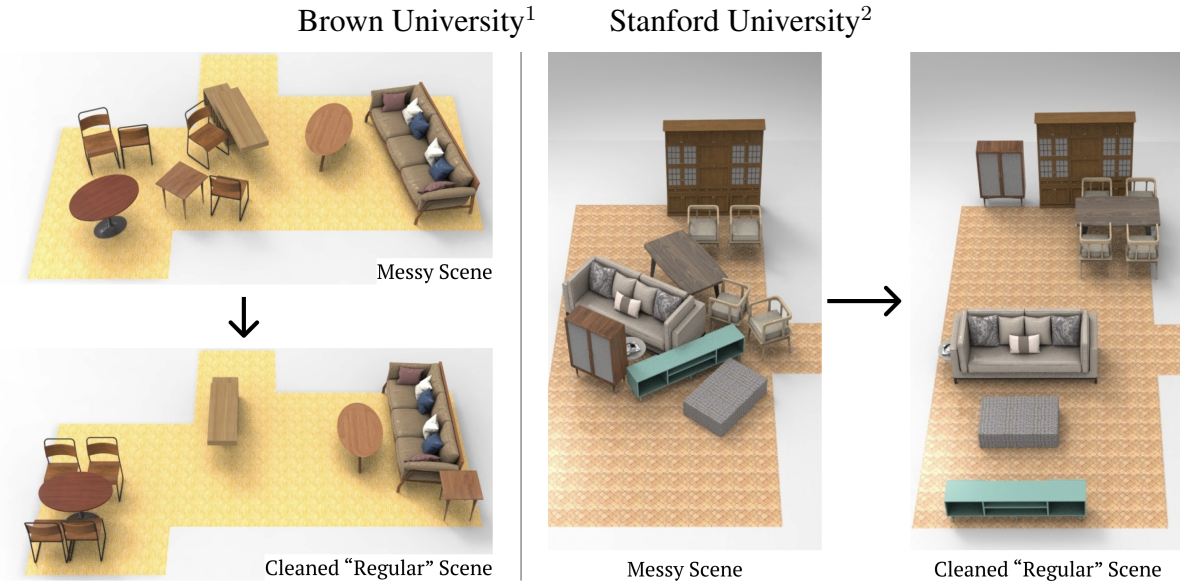


Figure 1. **LEGO-Net** **LE**arns to re**G**ularly rearrange **O**bjects in a messy indoor scene via an iterative denoising process. Different from scene synthesis or methods that require goal state specification, our method learns clean re-arrangements directly from data, retains the flavor of the original scene, and minimizes object travel distance. More about the project can be found at [ivl.cs.brown.edu/projects/lego-net](http://ivl.cs.brown.edu/projects/lego-net).

## Abstract

Humans universally dislike the task of cleaning up a messy room. If machines were to help us with this task, they must understand human criteria for regular arrangements, such as several types of symmetry, co-linearity or co-circularity, spacing uniformity in linear or circular patterns, and further inter-object relationships that relate to style and functionality. Previous approaches for this task relied on human input to explicitly specify goal state, or synthesized scenes from scratch – but such methods do not address the rearrangement of existing messy scenes without providing a goal state. In this paper, we present **LEGO-Net**, a data-driven transformer-based iterative method for **LE**arning re**G**ular rearrangement of **O**bjects in messy rooms. **LEGO-Net** is partly inspired by diffusion models – it starts with an initial messy state and iteratively “de-noises” the position and orientation of objects to a regular state while reducing distance traveled. Given randomly perturbed object positions and orientations

in an existing dataset of professionally-arranged scenes, our method is trained to recover a regular re-arrangement. Results demonstrate that our method is able to reliably re-arrange room scenes and outperform other methods. We additionally propose a metric for evaluating regularity in room arrangements using number-theoretic machinery.

## 1. Introduction

What makes the arrangement of furniture and objects in a room appear regular? While exact preferences may vary, humans have by-and-large universally shared criteria of regular room arrangements: for instance, heavy cabinets are arranged to align with walls, chairs are positioned evenly around a table in linear or circular configurations, or night stands are placed symmetrically on the two sides of a bed. Humans also share a common dislike of physically performing the task of rearranging a messy room. To build automated robotic systems that can guide or actually rearrange objects in a room, we first need methods that understand the shared human criteria for regular room rearrangements and

<sup>\*</sup>Core contribution.

respect the physical constraints of rearrangements.

Human criteria for regular rearrangements can be subtle and complex, including geometric rules of reflexional, translational, or rotational symmetry, linear or circular alignments, and spacing uniformity in object layout. Functional and stylistic inter-object relationships are also important: for example, a TV tends to be in front of and facing a sofa, chairs are next to a table or desk, etc. Many of these criteria interact and, at times, conflict with each other. As a result, in general, there is more than one desirable clean arrangement for any given messy arrangement. In our setting, we further desire that the clean rearrangement we create to be informed by the initial messy arrangement – and not be entirely different – for multiple reasons. First, there may have been a particular clean arrangement that gave rise to the messy one – and it may be desirable to recover a similar arrangement. Second, we want to minimize the motion of objects as much as possible to respect the physical constraints and effort involved – especially the motion of big and heavy furniture. Unfortunately, extant methods fail to capture these criteria: methods for scene synthesis from scratch [29, 34, 42, 73, 74, 76] ignore the initial state of objects in a room, and rearrangement methods often require scene-specific human input in the form of a goal state [1, 51] or language description [32, 52].

In this paper, we present LEGO-Net, a method for **LE**arning **reG**ular rearrangement of **O**bjects in rooms directly from data. Different from work that focuses on arranging new objects from scratch or requiring goal state specification, we focus on **rearranging** existing objects without any additional input at inference time. We take as input the position, orientation, class label, and extents of room objects in a specific arrangement, and output a room with the same objects but regularly re-arranged. LEGO-Net uses a transformer-based architecture [58] that is, in part, motivated by the recent denoising diffusion probabilistic models that learn a reverse diffusion process for generative modeling [19, 54, 55]. We learn human criteria for regular rearrangements from a dataset of professionally designed *clean* (regular) scenes [17], and represent each scene as a collection of objects and a floor plan. Prior to training, we perturb the arrangement of the regular scenes to generate noisy configurations. During training, our transformer learns to predict the original, de-noised scene arrangement from the perturbed arrangement and its floor plan. During inference, instead of directly re-arranging scenes with our model, which would amount to naïve regression, we run a Langevin dynamics-like reverse process to iteratively denoise object positions and orientations. This iterative process retains the flavor of original room state, while limiting object movement during re-arrangement.

We conduct extensive experiments on public datasets to show that our approach realistically rearranges noisy scene

arrangements, while respecting initial object locations. We also demonstrate that our method is able to generalize to previously unseen collection of objects in a wide variety of floor plan types. Furthermore, we include extensive experimental results (e.g., Fig. 1 and Fig. 4), including a new metric to evaluate regularity and symmetry of re-arrangements, aimed at measuring the presence of sparse linear integer relationships in the position of objects in the final state (using the PSLQ algorithm [15]). To sum up, we contribute:

- A generalizable, data-driven method that learns to **regularly re-arrange** the position and orientation of objects in different kinds of messy rooms.
- An iterative approach to re-arrangement at inference time that retains flavor of the original arrangement and minimizes object travel distance.
- An in-depth analysis of the performance and characteristics of the denoising-based scene rearrangement.
- A new metric to measure the regularity of object arrangement based on integer relation algorithms.

## 2. Related Work

In this section, we discuss literature in two related areas: (1) scene synthesis from scratch, (2) scene rearrangement where an end goal is specified, and (3) diffusion models.

**Indoor 3D Scene Synthesis:** Indoor room synthesis is the problem of synthesizing the layout of objects in a scene from scratch. Many classical methods in the computer graphics literature use heuristics and guidelines to constrain the location of pre-specified objects [6, 67, 68, 71]. [36] identified a collection of functional, visual, and design constraints and formulate an optimization problem. Work has also focused exclusively on inter-object relationships [30]. Other methods [69] address the open world layout problem when objects are not pre-specified.

An alternative approach is to adopt procedural modeling using generative grammars [5, 7, 10, 40, 42, 57]. Some methods adopt the scenegraph representation and formulate it as a graph problem [29, 34, 38, 62, 73, 74, 76]. Both procedural and graph-based methods often rely on curated data [16]. Some methods learn directly from data using neural networks, for instance from images [44]. Both SceneFormer [65] and ATISS [39] introduce autoregressive methods for scene generation. Different from all these methods, our approach is to *rearrange* rooms given an initial messy arrangement.

**Scene Rearrangement:** In scene rearrangement, the task is to take an initial state of the scene and bring it to a goal state which is specified by the user. This task is deeply connected to planning in robotics [1, 47, 53]. Some works consider robot pushing and manipulation for rearrangement [2, 8, 9, 13, 23, 24, 26, 27, 50, 51]. Many of these methods require datasets for training and often use datasets

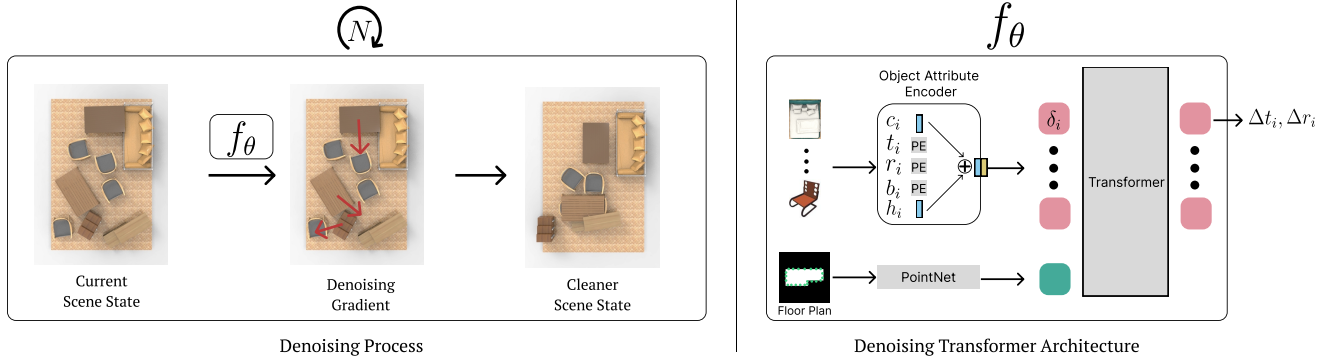


Figure 2. Pipeline overview. LEGO-Net takes an input messy scene and attempts to clean the scene via iterative denoising. Given the current scene state, it computes the denoising gradient towards the clean manifold, and makes changes to the scene accordingly. This denoising step is taken repeatedly until the scene is “regular.” On the right, we show our backbone transformer block  $f_\theta$  that computes the denoising gradient at each step. This transformer takes the scene attributes of the current state and outputs 2D transformations of each object that would make the scene “cleaner”.

like AI2-THOR [25], Habitat [56] or Gibson [28]. Some of these methods operate on visual observations [23], while others assume fully-observed synthetic environments [8]. To specify the goal state, some recent methods use language input [32, 52] driven by large language models [11, 43]. Related to these advances in robotics, there have also been attempts to apply these specifically for room rearrange-ments [61, 66].

In this paper, we focus on the task of room rearrange-ments without the need to specify the goal state. We directly learn arrangements that satisfy human criteria from profes-sionally arranged dataset provided by 3D-FRONT [17].

**Denoising Diffusion Models:** 2D Diffusion models [19, 54, 55] have emerged as a powerful technique for uncondi-tional image synthesis, outperforming existing 2D generative models [14, 22]. Diffusion models have also seen great success in conditional image generations, receiving condi-tions in the form of class labels [12], text [37, 45], or input images [48]. Various methods [33, 35, 48] apply diffusion models for *restoring* corrupted or user-provided images into realistic images. Our method shares the same philosophy and adopts related techniques from the diffusion models, e.g., Langevin Dynamics, to project messy object configu-rations onto the manifold of “clean” scenes.

### 3. Method

#### 3.1. Preliminaries

Our method takes the position, orientation, class label, and extents of objects in a ‘messy’ room as input and out-puts a rearranged version in a ‘regular’ state. Since objects in rooms primarily move on the floor, we only consider 2D object pose, but our method can be combined with existing instance segmentation [64, 70] and canonicalization meth-ods [49] to directly operate from a 3D mesh or point cloud. We represent each scene  $X$  as an unordered set of  $n$  objects

and their transformations:

$$X = \{o_1, \dots, o_n\}, \quad o_i = (c_i, t_i, r_i, b_i, h_i), \quad (1)$$

where  $c_i \in \mathbb{R}^k$ ,  $t_i \in \mathbb{R}^2$ ,  $r_i \in SO(2)$ , and  $b_i \in \mathbb{R}^2$  respec-tively denote the semantic class, translation, rotation, and bounding box dimensions of the object  $o_i$ . Here,  $h_i \in \mathbb{R}^{128}$  is the pose-canonicalized shape features both obtained by running ConDor [49] on each object’s point cloud (see sup-plementary for the process). The furniture semantic class la-bels  $c_i$ ’s are represented as one-hot vectors of the  $k$  classes. We represent the rotation  $r_i \in SO(2)$  by the first col-umn vector  $[\cos(\theta), \sin(\theta)]^\top$  of its rotation matrix, follow-ing [75] to represent  $SO(2)$  without any discontinuity. Note that  $t_i$  is normalized to be in  $[-1, 1]$  to have the same range as  $r_i$ ’s sinusoidal representation to balance their importance during training. We define that a scene  $X^a$  is a rearrange-ment of  $X^b$  (denoted  $X^a \sim X^b$ ) iff there exists a bijection  $\rho$  between object indices such that  $h_i^a \approx h_{\rho(i)}^b$ .

#### 3.2. LEGO-Net: Learning Regular Room Rear-rangements

Fig. 2 shows our approach to solving the regular room rear-rangement problem. Our method takes an input ‘messy’ scene  $\tilde{X}$  and outputs a rearranged, ‘regular’ scene  $X$ . To-wards this goal, we design a denoising Transformer [58]  $f_\theta$  that is trained to predict a clean scene given its perturbed version. During inference, we take an iterative approach because it gives us rich control of the rearrangement pro-cess, e.g., moving lighter objects farther. At each time step  $\tau$  of the denoising process, we pass the current scene state  $\tilde{X}_\tau$  to the denoising Transformer  $f_\theta$  that provides gradients towards the manifold of ‘clean’ scenes. We repeat the op-timization process until the magnitude of the predicted gra-dient is small enough to finally obtain a clean manifold pro-jection of the input scene.

**Manifold Projection via Denoising Autoencoder:** We now describe our approach from a manifold learning perspective. We can consider the input to our method as an off-manifold point  $\tilde{X}$  (i.e., a messy scene) and aim to project it to the closest point  $X$  on the manifold of ‘regular’ scenes. Our objective is to learn a function  $f_\theta(\tilde{X})$  (with network parameters  $\theta$ ) that finds such manifold projected point  $X$ , i.e.,  $f_\theta(\tilde{X}) \approx X$ . Motivated by the denoising autoencoders [60] and their recent extensions to score-matching models [19, 54], we train such  $f(\tilde{X})$  by perturbing the regular data  $X$  employing a noise kernel  $q_\sigma(\tilde{X}|X)$  with noise parameter  $\sigma$ . The training is done by minimizing a denoising objective function:

$$\mathcal{E}_{dn}(\theta) = \mathbb{E}_{q_\sigma(\tilde{X}, X)} \left[ \mathcal{L}_{dn} \left( f_\theta(\tilde{X}), X \right) \right]. \quad (2)$$

The joint distribution  $q_\sigma(\tilde{X}, X) = n(\sigma)q_\sigma(\tilde{X}|X)q_0(X)$ , where  $n(\sigma)$  is the distribution of the noise parameter and  $q_0(X)$  is the discrete uniform distribution of the training examples. Here, the loss  $\mathcal{L}_{dn}$  is defined as the average distance between the pairs of objects in  $f_\theta(\tilde{X})$  and  $X$ :

$$\mathcal{L}_{dn} = \frac{1}{n} \sum_{i=0}^n \left( \|\tilde{t}_i - t_i\|_2^2 + \|\tilde{r}_i - r_i\|_2^2 + \lambda_1 (\|\tilde{t}_i - t_i\|_1 + \|\tilde{r}_i - r_i\|_1) \right), \quad (3)$$

where  $\tilde{t}_i$  and  $\tilde{r}_i$ ’s are the object rotation and translation parameters of  $f_\theta(\tilde{X})$ , and  $\lambda_1$  is a balancing parameter for the L1 loss. While we can use the object correspondences from the perturbation process, we choose to reassociate the correspondences by computing Earth Mover’s Distance [46] between the same class of objects in the two scenes.

Intuitively, the network  $f_\theta(\tilde{X})$  learns to project  $\tilde{X}$  to the clean manifold. However, it is not trained to find a random point in the clean manifold, but rather tries to find  $X$  that shares similarities to  $\tilde{X}$ , depending on the noise level.

**Connection to Score-based Models:** While the trained denoising network  $f_\theta$  can theoretically be applied to clean up a messy scene, in practice, the quality of the output is suboptimal, as shown in Sec. 4. This is because the network  $f_\theta$  is trained with a *regression* loss, which is known to fit to the average state of the conditional distribution  $q_\theta(X|\tilde{X})$ , leading to blurry predictions [21, 72].

Recently, score-based generative models (and the closely related diffusion models) [19, 54] have shown impressive image generation results using a trained denoiser. The score-based approaches [54, 59] approximate the gradient of likelihood of the perturbed data distribution  $q_\sigma(\tilde{X})$  with a neural network  $s_\phi$ , and showed that the optimal network  $s_\phi^*$  for the denoising objective  $\mathbb{E}_{q_\sigma(\tilde{X}, X)} \left[ \left\| s_\phi(\tilde{X}) - \nabla_{\tilde{X}} \log q_\sigma(\tilde{X}|X) \right\|^2 \right]$  satisfies  $s_\phi^*(\tilde{X}) \approx \nabla_{\tilde{X}} \log q_\sigma(\tilde{X})$ . Assuming a zero-mean Gaussian

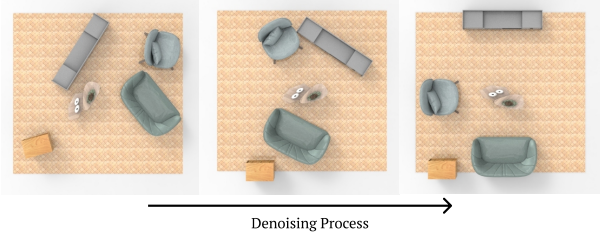


Figure 3. Rather than directly regressing the final rearranged state which can lead to non-diverse results, we adopt an iterative strategy based on Langevin Dynamics. At each step in our process (left to right), we gradually “de-noise” the scene until it reaches a regular state. During training, we follow the reverse process, i.e., perturb clean scenes to messy state (right to left).

noise kernel  $q_\sigma(\tilde{X}|X)$ , the score-based network training objective becomes:

$$\mathcal{L}_{score}(\phi) = \mathbb{E}_{q_\sigma(\tilde{X}, X)} \left[ \left\| s_\phi(\tilde{X}) - \frac{X - \tilde{X}}{\sigma^2} \right\|^2 \right]. \quad (4)$$

Since the trained score network  $s_\phi^*$  approximates the gradient of the data distribution,  $s_\phi^*(\tilde{X})$  can be used for autoregressively optimizing a noisy data onto the manifold of clean data. In our context,  $X - \tilde{X}$  amounts to the difference in object transformations between the clean and perturbed scenes, and the direction  $\frac{X - \tilde{X}}{\sigma^2}$  predicted by  $s_\phi^*(\tilde{X})$  is clearly towards the clean scene manifold.

**Rearrangement with Langevin Dynamics:** After the training of Eq. 2, we have a function that is optimized to approximate the denoised projection of an input, i.e.,  $f_\theta^*(\tilde{X}) \approx X$ . Given that  $s_\phi^*(\tilde{X}) \approx \frac{X - \tilde{X}}{\sigma^2}$ , we have that  $s_\phi^*(\tilde{X}) \propto f_\theta^*(\tilde{X}) - \tilde{X}$ . We then follow the score-based methods to adopt the Langevin dynamics [19, 54] to recursively denoise the scene (see Fig. 3) using the estimated gradients:

$$\tilde{X}_{\tau+1} = \tilde{X}_\tau + \alpha(\tau) \left( f_\theta^*(\tilde{X}_\tau) - \tilde{X}_\tau \right) + \beta(\tau) z_\tau, \quad (5)$$

where  $\alpha(\tau)$  and  $\beta(\tau)$  are monotonically-decreasing functions of time  $\tau$  that is heuristically designed to balance the Langevin dynamics, and  $z_\tau \sim \mathcal{N}(0, 1)$ . Here, the transformation of  $o_i^{a-b}$  in  $X^a - X^b$  is the relative transformation between the corresponding objects:  $t_i^a - t_i^b$  and  $r_i^a \bar{r}_i^b$ . We run the recursive computation until the magnitude of the gradient is small enough (i.e.,  $\|f_\theta^*(\tilde{X}_{\tau_i}) - \tilde{X}_{\tau_i}\| < \kappa$ , for constant  $\kappa$ ) for 5 consecutive iterations.

### 3.3. Architecture

LEGO-Net follows the recent success in the scene synthesis community to adopt the Transformer architecture [58] to represent our denoising function  $f_\theta$ , as illustrated in Fig. 2. Given an input scene  $\tilde{X}$ , a Transformer



encoder network,  $F_\theta$ , takes in  $|\tilde{X}| + 1$  number of 512-dimensional tokens  $\delta_i$ 's corresponding to the objects in the scene, as well as the room background layout. Then, the network outputs absolute translation and rotation predictions for all object tokens (excluding the layout token), i.e.,  $F_\theta : \mathbb{R}^{(|\tilde{X}|+1) \times 512} \mapsto \mathbb{R}^{|\tilde{X}| \times 4}$ . We then apply the outputs to translate and rotate each object in  $\tilde{X}$ . The denoiser  $f_\theta$  is defined to include both operations. Therefore, the processed scene is a rearrangement of the input scene:  $f_\theta(\tilde{X}) \sim \tilde{X}$ .

**Input Object Attribute Encoding:** We use the following process to abstract  $o_i$  into a token vector  $\delta_i$ . We employ positional encodings of 32 frequencies, and an additional linear layer for  $r_i$ , to independently process  $t_i, r_i, b_i$  into 128-dimensional vectors. For object class  $c_i$ , we employ a 2-layer MLP with leaky ReLU activation to process the one-hot encoding into a 128-dimensional attribute. Finally, we optionally process a pose-invariant shape feature  $h_i$  from ConDor [49] with a 2-layer MLP to obtain a 128-dimensional feature. The above attribute features are then concatenated and processed with a 2-layer MLP to form an object token  $\delta_i \in \mathbb{R}^{512}$ . We refer readers to supplementary for the full details of the processing.

**Floor Plan Encoder:** Floor plans designating room boundaries both impose important realistic constraints and provide regularity information for the scene rearrangement task. Therefore, we pass the room layout in the form of an object token to the transformer so that other objects can attend to it. We employ a floor plan encoder to tokenize the floor plans as follows. We uniformly sample 250 points from the contour of the floor plan along with the 2D surface normal of these points. These points are then processed with a simplified version of PointNet [41]. Finally, we specifically assign one bit of the 512 transformer input dimensions (for both objects and floor plans) to distinguish floor plan ‘objects’ from normal ‘objects’. The final output of the floor plan encoder for each scene is a  $\mathbb{R}^{512}$  feature.

**Transformer Architecture:** We use our custom positional encodings and procedures to prepare the tokens but use the original Transformer encoder architecture without notable modifications. We use 8 multi-headed attentions with 512 dimensional hidden layers and 512 dimensional key, query, and value vectors. The output of the transformer network is the estimated object transformations, a  $|X| \times 4$  matrix.

### 3.4. Training and Inference

**Data:** We employ the 3D-FRONT dataset [17] for the task of indoor scene rearrangement. For each valid clean scene in the dataset, we preprocess it into  $X = \{o_1, \dots, o_n\}$  and extract the contour of its floor plan.

**Training:** We use the denoising auto-encoder formulation of Eq. 2 to train our denoiser function  $f_\theta$ . We uniformly randomly sample training examples and sample a noise level  $\sigma$

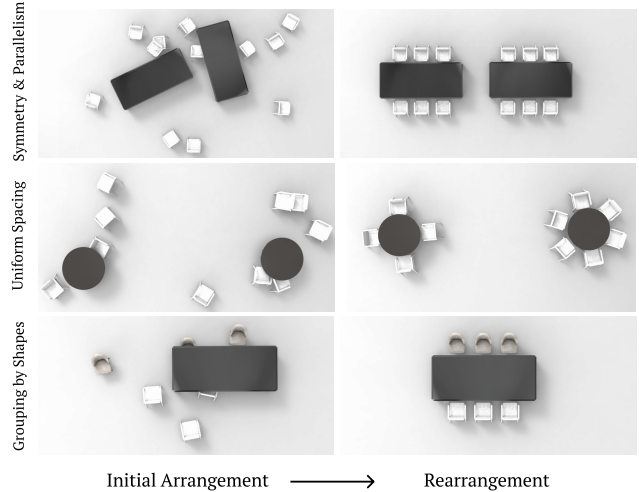


Figure 4. Regularities learning results. We train our denoising network to learn three different regularities. LEGO-Net successfully learns the complex regularity rules as demonstrated by the iterative denoising results shown in the right.

from a normal distribution. The sampled examples are perturbed using an independent Gaussian kernel with standard deviation  $\sigma$ . For the perturbation, we do not consider objects going outside of the floor plans or colliding with each other. Each perturbed scene uses its original clean scene as the source of ground truth but re-establishes object correspondence through Earth Mover’s Distance assignment to enable invariance among identical objects and further promote distance minimization in movement prediction. We use Adam optimizer to train our model to minimize the training objective with a learning rate of  $10^{-4}$ .

**Inference:** During inference, we use the Langevin Dynamics scheme of Eq. 5 to iteratively project a messy scene input  $\tilde{X}$  onto the manifold of clean scenes. We select a hyperbolic function  $\alpha(\tau) = \alpha_0 / (1 + a_1 * \tau)$  to regulate the step size. We additionally select an exponential  $\beta(\tau) = \beta_0 * b_1^{\lfloor \tau / b_2 \rfloor}$ , where effectually  $\beta_0$  is multiplied by  $b_1$  every  $b_2$  iterations, to adjust the level of noise as the denoising process proceeds. Refer to supplementary for details.

## 4. Experiments

We conduct a number of experiments to test LEGO-Net’s ability to automatically capture scene regularities from data. To this end, we prepare two testbeds for experiments: First is our custom-designed **Table-Chair** environment where we mathematically design the regularities between the objects. Second is **3D-Front** [17], which contains tens of thousands of synthetic rooms designed by professionals. The Table-Chair dataset is useful because we can model one regularity at a time and quantify network performance. 3D-Front dataset exhibits complex and subtle rules that design-



Figure 5. Comparison against ATISS [39] on 3D-front dataset. Being the state-of-the-art scene synthesis method, ATISS is able to produce a realistic scene (3rd column) given the floor plan of the ground truth, but the generated objects and arrangements are totally different. On the other hand, we solve the problem of re-arranging the given messy scene, directly using the existing objects in the scene. While ATISS, in their paper, has shown failure correction technique that solves similar problem to ours, we observe that when the scene is highly noisy their algorithm tends to deteriorate significantly. Moreover, being an one-shot prediction type method, ATISS-failure does not consider the moving distance of the new configurations.

ers commonly perceive as ideal configurations, *e.g.*, geometry, semantic relations, styles, and functionalities.

#### 4.1. Capturing Regularities from Data

In the Table-Chair environment, we study four main regularities: symmetry, parallelism, uniform spacing, and grouping by shapes. For each of the proposed experiments, we generate clean scenes based on the designed rules. Then, for training, we perturb the scenes on the fly to generate clean-messy pairs. We then re-associate objects within each class through Earth Mover’s Distance assignment to finally train a network with the loss of Eq. 2. We measure each task with the success rate of the rearrangement, whose specific criteria we discuss in the supplementary.

**Symmetry and Parallelism:** One of the most important notions of regular arrangement is symmetry, which involves both object-object symmetries and room-level symmetries. We use a setting with 2 groups of rectangular tables and chairs. We designate the 2 tables to be vertically aligned and distribute them horizontally at a distance uniformly drawn from a fixed range. We arrange 3 chairs in a linear row on one side of the table and 3 chairs in another linear row on the opposite of the table, in perfect symmetry and parallelism with each other (first row of Fig. 4).

**Uniform Spacing:** We prepare a highly-challenging setup to stress test LEGO-Net’s ability to capture the concept of uniform spacing. In this setup, we have two circular tables, and each of them has 2–6 chairs randomly rotated around them with uniform distances between each pair. The networks have to deal with the unknown number of chairs and their distances.

**Grouping by Shape:** We test LEGO-Net’s ability to group objects based on their pose-invariant shapes. We augment our setup in “symmetry and parallelism” to include two types of chairs with different shapes. We arrange the scenes such that chairs with the same shapes are on the same side of the table. The pose-invariant shape features  $h_i \in o_i$  from

	Symmetry & Parallelism $\uparrow$	Uniform Spacing $\uparrow$	Grouping by Shape $\uparrow$
Direct	16%	18.6%	23.6%
Grad. w/o noise	91.2%	96%	87.8%
Grad. w/ noise	<b>91.4%</b>	<b>97.2%</b>	<b>89.2%</b>

Table 1. Denoising success rate by regularities and inference strategies. For the three regularities shown in Fig. 4, we measure the success rate of LEGO-Net for each of the inference variants.

Eq. (1) provides the necessary shape information.

**Results:** We visualize samples of the rearrangement performed by LEGO-Net on the three above environments in Fig. 4. Across the board, the denoising network successfully learns to capture these important regularities from data, without explicit supervision about the underlying rules. The success rates of each task are shown in Tab. 1. As expected, directly applying the regression-trained network  $f_\theta$  results in worse results.

#### 4.2. 3D-Front Experiments

We benchmark LEGO-Net’s ability to conduct regular scene rearrangements on the bedrooms and living rooms of the 3D-Front dataset, each of them containing 2338/587 and 5668/224 train/test splits. The task for LEGO-Net on this dataset is to denoise the input perturbed scenes.

We train our LEGO-Net following the procedures described in Sec. 3 with  $\sigma \sim \mathcal{N}(0, 0.1^2)$ . While we maintain a single denoising network  $f_\theta$ , we explore three variants of inference algorithms to provide greater insight of our approach: (1) LEGO-Net *direct*, (2) *grad. with noise*, and (3) *grad. w/o noise*, respectively denotes the inference strategy of predicting the clean outcome with one network pass, running Langevin Dynamics of Eq. (5) with non-zero, and zero noise term  $\beta$ .

**Baselines.** We compare our rearrangement results against

the current SOTA scene synthesis method, ATISS [39]. While ATISS is designed to synthesize a scene from scratch rather than to rearrange one, it provides an auto-regressive generative model that can be flexibly applied to our task. Specifically, we use three variants of ATISS that share the same network weights. First, ATISS *vanilla* performs its original scene synthesis task given a floor plan. Second, ATISS with *labels* performs object placements using a pre-defined set of objects to place per scene. Third, ATISS *failure-correction* takes a noisy scene and cleans it up by iteratively finding an object with low probability and replacing them within the current scene. This variant of ATISS is given the same perturbed scene as LEGO-Net and aims at cleaning the scene. Note that we omit to compare against prior works that have already been compared against ATISS, e.g., [44, 62, 65]. We could not find a prior data-driven method that is designed to solve the same rearrangement problem as ours.

**Metrics.** To gauge how accurately our method captures regularities within the dataset, we adopt the popular FID and KID scores. These metrics compare the statistics of two data distributions and measure their closeness. We follow prior works [39, 63] to render ground truth and generated scene arrangements from top-down view and compute the metrics in the image space. Among the two metrics, KID is more applicable to our setting, because FID is known to present huge bias when the number of data is low. Another important criterion for our rearrangement task is how much distance the objects have to be moved from the initial to the final scene state. Similarly, when applicable, we measure the Earth Mover’s Distance (EMD) between the ground truth scene and our cleaned-up scene, to gauge how accurately the denoising predictions were made.

Finally, we introduce a new metric based on integer relations to measure regularities by finding integer relations between object coordinates  $t_i$ ’s. See supplementary for detailed descriptions of metrics.

**Results.** We conduct the 3D-Front arrangement experiments with five algorithms (three ATISS variants and two of ours) and compute their metrics. The numerical results, which can be found in Tab. 2, show that LEGO-Net outperforms all variants of ATISS, including the failure-correction variant that tackles the same object cleaning problem as demonstrated in the original paper.

Moreover, we measure the scene regularities by finding integer relations between object coordinates  $t_i$ ’s. To do this, we select two or three random objects within a scene and check if we can find non-zero integers  $a_i$ ’s that satisfy

$$a_1 t_1 + \dots + a_n t_n = 0, \quad 0 < |a_i| < \eta, \forall a_i \quad (6)$$

where  $\eta$  sets the maximum magnitude of the coefficients. Intuitively, these integer relations can capture regularities such as colinearities ( $-t_1 + t_2 = 0$ ) and symmetries

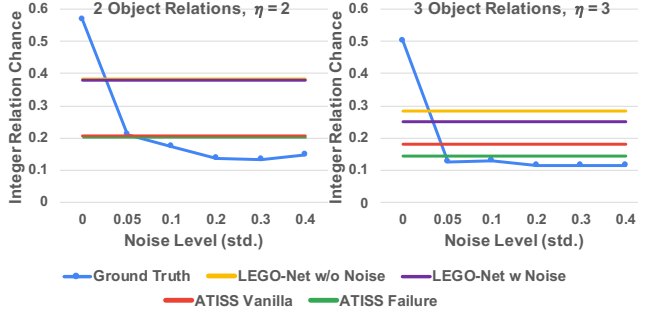


Figure 6. Integer relation occurrences. We measure the chance of finding integer relations between the coordinates of two (left) and three (right) objects within a Living Room scene. Perturbing ground truth scenes sharply decreases the integer relation occurrences, showing they are useful metric of regularities. Note that LEGO-Net outperforms ATISS variants in this metric.

( $t_1 - 2t_2 + t_3 = 0$ ). In Fig. 6, we plot the chance of finding integer relations in scenes perturbed with different noise levels, which peaks for the original clean 3D-FRONT scenes and sharply decreases as noise is added. Also, note that the rearranged scenes of LEGO-Net demonstrate high regularities according to this measure, outperforming the results of ATISS variants. See supplementary for details.

Qualitatively, as shown in Fig. 5, LEGO-Net is able to robustly project messy scenes onto clean manifolds. While ATISS and ATISS with *labels* were able to synthesize realistic rooms, their object arrangements have nothing to do with the original input. Importantly, we notice that ATISS failure correction leads to unexpectedly low-quality results. We hypothesize that this is due to their discrete, one-object-at-a-time strategy, which can easily fall into the local minimum of the likelihood space. In contrast, our score-based iterative denoising leads to robust success rates.

### 4.3. Analysis

To more deeply understand the behavior of our system we analyze and discuss important aspects of LEGO-Net. We refer to supplementary for more analysis of our method.

**Denosing Strategy.** As we discuss throughout Sec. 4, we explore three inference strategies, namely, direct, gradient with noise, and gradient without noise. For the 3D-Front experiment, we report that the *grad. without noise* variant consistently outperforms the other variant. However, we believe that this is likely because we used relatively low noise to the scenes (std 0.1) to simulate more naturally messy indoor rooms. Indeed, our experiment on the synthetic environment (Tab. 1) with larger noise (std 0.25) shows that the *grad. with noise* variant outperforms. The results suggest that adding noise during Langevin dynamics allows a better success rate for highly noisy data, but at the cost of losing accuracy in recovering the originals (as shown in Tab. 2).

		Living Room				Bedroom			
		KID↓	FID↓	Distance↓ Moved	EMD ↓ to GT	KID↓	FID↓	Distance↓ Moved	EMD ↓ to GT
ATISS [39]	<i>vanilla</i>	96	44.55	—	—	33	50.49	—	—
	<i>labels</i>	119	45.45	—	0.3758	49	52.62	—	0.5482
	<i>failure-correction</i>	280	61.55	0.1473	0.3378	240	73.95	0.2025	0.4673
LEGO-NET (ours)	grad. w/ noise	67	39.19	0.091	0.125	37	49.76	0.052	0.086
	grad. w/o noise	<b>51</b>	<b>37.47</b>	<b>0.086</b>	<b>0.117</b>	<b>27</b>	<b>48.43</b>	<b>0.0492</b>	<b>0.0815</b>

Table 2. Quantitative experiment results using KID  $\times 10,000$ , FID, distance moved, and Earth Mover’s Distance (EMD) against the ground truth arrangements. All scenes are situated within  $[-1, 1]^2$  canvas. Note that ATISS *vanilla* and *fixed labels* version start from empty floor plans and thus distance moved metric is not applicable. ATISS *failure-correction* takes a noisy scene and iteratively resamples low-probable objects, and thus is directly comparable to our method.

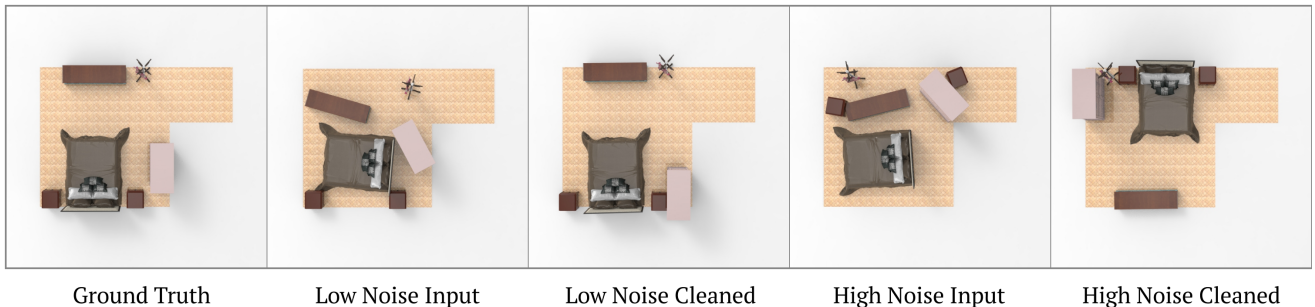


Figure 7. LEGO-Net denoising results on different noise levels. When the perturbation added to the scene is low, LEGO-Net is able to closely reconstruct the clean version of the scene. In contrast, when the noise level is high, our denoising process finds a different realization of a regular scene, behaving more like an unconditional model. Similar phenomena have been observed by 2D diffusion projects, e.g., SDEdit [35].

**Cleaning Uncertainty.** LEGO-Net is trained to handle input perturbations at various noise levels. In the high-noise regime, there is high uncertainty on the structure of the original information. As input noise increases, our denoising process converges into an unconditional generative model. On the other hand, LEGO-Net has the capacity to capture original regularities when the noise is low, leading to almost precisely reconstructing the original scene. We visually show these insights in Fig 7.

**Out-of-Distribution Inputs.** We showcase LEGO-Net’s ability to handle scenes perturbed with noise patterns very different from the one used in training, *i.e.*, zero-mean Gaussian. In the first example, we only perturb chairs in the scene. Secondly, we perturb the scene only in the translation dimensions without rotations. Shown in Fig. 8, LEGO-Net can successfully handle out-of-distribution inputs, demonstrating the robustness and versatility of our algorithm.

## 5. Conclusion

In this paper, we presented LEGO-Net, a method for regular rearrangement of objects in a room. Different from previous methods, LEGO-Net learns human notions of regularity (including symmetry, stylistic and functional

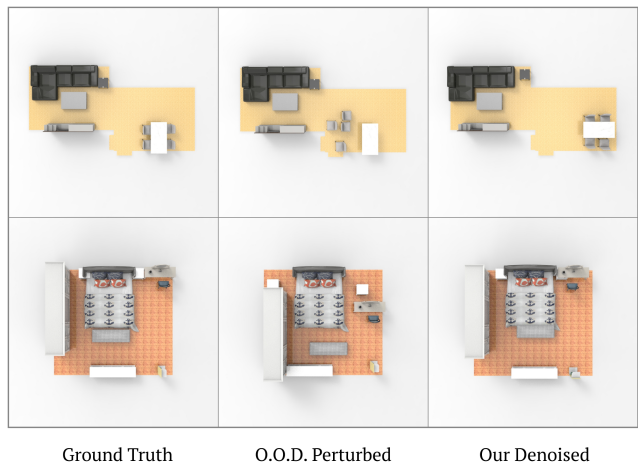


Figure 8. Out-of-distribution test. While our model is trained to denoise Gaussian noise, it demonstrates strong robustness to out-of-distribution inputs. In the first row, only the chairs are perturbed. For the second row, we perturbed the scene with translation noise only. Zoom-in for details.

factors) directly from data without the need to explicitly specify a goal state. During training, we learn from a large dataset of professionally-designed room layouts that



are randomly perturbed. During inference, we follow a Langevin Dynamics-like strategy to iteratively “denoise” the scene. Quantitative results including comparisons and ablations show that our method performs well which qualitative results confirm.

**Limitations & Future Work:** Our method has important limitations that provide extensive opportunities for future work. First, our method is currently limited to 2D room rearrangement and cannot perform 3D rearrangement, for instance in kitchen shelves. However, we do incorporate 3D shape features which can be used to extend our method to 3D. We also currently do not handle interpenetration of objects during denoising which future work should explore.

## Acknowledgements

This work was supported by AFOSR grant FA9550-21-1-0214, NSF CloudBank, an AWS Cloud Credits award, ARL grant W911NF-21-2-0104, a Vannevar Bush Faculty Fellowship, and a gift from the Adobe Corporation. We thank Kai Wang, Daniel Ritchie, Rao Fu, and Selene Lee.

## References

- [1] Dhruv Batra, Angel X Chang, Sonia Chernova, Andrew J Davison, Jia Deng, Vladlen Koltun, Sergey Levine, Jitendra Malik, Igor Mordatch, Roozbeh Mottaghi, et al. Rearrangement: A challenge for embodied ai. *arXiv preprint arXiv:2011.01975*, 2020. [2](#)
- [2] Ohad Ben-Shahar and Ehud Rivlin. Practical pushing planning for rearrangement tasks. *IEEE Transactions on Robotics and Automation*, 14(4):549–565, 1998. [2](#)
- [3] Paul J Besl and Neil D McKay. Method for registration of 3-d shapes. In *Sensor fusion IV: control paradigms and data structures*, volume 1611, pages 586–606. Spie, 1992. [14](#)
- [4] Miłkołaj Bińkowski, Danica J Sutherland, Michael Arbel, and Arthur Gretton. Demystifying mmd gans. *arXiv preprint arXiv:1801.01401*, 2018. [14](#)
- [5] Martin Bokeloh, Michael Wand, Hans-Peter Seidel, and Vladlen Koltun. An algebraic model for parameterized shape editing. *ACM Transactions on Graphics (TOG)*, 31(4):1–10, 2012. [2](#)
- [6] Richard W Bukowski and Carlo H Séquin. Object associations: a simple and practical approach to virtual 3d manipulation. In *Proceedings of the 1995 symposium on Interactive 3D graphics*, pages 131–ff, 1995. [2](#)
- [7] Siddhartha Chaudhuri, Daniel Ritchie, Jiajun Wu, Kai Xu, and Hao Zhang. Learning generative models of 3d structures. In *Computer Graphics Forum*, volume 39, pages 643–666. Wiley Online Library, 2020. [2](#)
- [8] Akansel Cosgun, Tucker Hermans, Victor Emeli, and Mike Stilman. Push planning for object placement on cluttered table surfaces. In *2011 IEEE/RSJ international conference on intelligent robots and systems*, pages 4627–4632. IEEE, 2011. [2](#), [3](#)
- [9] Michael Danielczuk, Andrey Kurenkov, Ashwin Balakrishna, Matthew Matl, David Wang, Roberto Martín-Martín, Animesh Garg, Silvio Savarese, and Ken Goldberg. Mechanical search: Multi-step retrieval of a target object occluded by clutter. In *2019 International Conference on Robotics and Automation (ICRA)*, pages 1614–1621. IEEE, 2019. [2](#)
- [10] Jeevan Devaranjan, Amlan Kar, and Sanja Fidler. Meta-sim2: Unsupervised learning of scene structure for synthetic data generation. In *European Conference on Computer Vision*, pages 715–733. Springer, 2020. [2](#)
- [11] Jacob Devlin, Ming-Wei Chang, Kenton Lee, and Kristina Toutanova. Bert: Pre-training of deep bidirectional transformers for language understanding. *arXiv preprint arXiv:1810.04805*, 2018. [3](#)
- [12] Prafulla Dhariwal and Alexander Nichol. Diffusion models beat gans on image synthesis. *Advances in Neural Information Processing Systems*, 34:8780–8794, 2021. [3](#)
- [13] Mehmet R Dogar, Michael C Koval, Abhijeet Tallavajhula, and Siddhartha S Srinivasa. Object search by manipulation. *Autonomous Robots*, 36(1):153–167, 2014. [2](#)
- [14] Patrick Esser, Robin Rombach, and Bjorn Ommer. Taming transformers for high-resolution image synthesis. In *Proceedings of the IEEE/CVF conference on computer vision and pattern recognition*, pages 12873–12883, 2021. [3](#)
- [15] Helaman R. P. Ferguson and David H. Bailey. A polynomial time, numerically stable integer relation algorithm. *Number RNR-91-032*, 1991. [2](#), [17](#)
- [16] Matthew Fisher, Daniel Ritchie, Manolis Savva, Thomas Funkhouser, and Pat Hanrahan. Example-based synthesis of 3d object arrangements. *ACM Transactions on Graphics (TOG)*, 31(6):1–11, 2012. [2](#)
- [17] Huan Fu, Bowen Cai, Lin Gao, Ling-Xiao Zhang, Jiaming Wang, Cao Li, Qixun Zeng, Chengyue Sun, Rongfei Jia, Bin-qiang Zhao, et al. 3d-front: 3d furnished rooms with layouts and semantics. In *Proceedings of the IEEE/CVF International Conference on Computer Vision*, pages 10933–10942, 2021. [2](#), [3](#), [5](#), [12](#), [14](#)
- [18] Martin Heusel, Hubert Ramsauer, Thomas Unterthiner, Bernhard Nessler, and Sepp Hochreiter. Gans trained by a two time-scale update rule converge to a local nash equilibrium. *Advances in neural information processing systems*, 30, 2017. [14](#)
- [19] Jonathan Ho, Ajay Jain, and Pieter Abbeel. Denoising diffusion probabilistic models. *Advances in Neural Information Processing Systems*, 33:6840–6851, 2020. [2](#), [3](#), [4](#), [15](#)
- [20] Alain Hore and Djemel Ziou. Image quality metrics: Psnr vs. ssim. In *2010 20th international conference on pattern recognition*, pages 2366–2369. IEEE, 2010. [15](#)
- [21] Phillip Isola, Jun-Yan Zhu, Tinghui Zhou, and Alexei A Efros. Image-to-image translation with conditional adversarial networks. In *Proceedings of the IEEE conference on computer vision and pattern recognition*, pages 1125–1134, 2017. [4](#)
- [22] Tero Karras, Miika Aittala, Janne Hellsten, Samuli Laine, Jaakko Lehtinen, and Timo Aila. Training generative adversarial networks with limited data. *Advances in Neural Information Processing Systems*, 33:12104–12114, 2020. [3](#)
- [23] Jennifer E King, Marco Cognetti, and Siddhartha S Srinivasa. Rearrangement planning using object-centric and

- robot-centric action spaces. In *2016 IEEE International Conference on Robotics and Automation (ICRA)*, pages 3940–3947. IEEE, 2016. 2, 3
- [24] Jennifer E King, Vinitha Ranganeni, and Siddhartha S Srinivasa. Unobservable monte carlo planning for nonprehensile rearrangement tasks. In *2017 IEEE International Conference on Robotics and Automation (ICRA)*, pages 4681–4688. IEEE, 2017. 2
- [25] Eric Kolve, Roozbeh Mottaghi, Winson Han, Eli VanderBilt, Luca Weihs, Alvaro Herrasti, Daniel Gordon, Yuke Zhu, Abhinav Gupta, and Ali Farhadi. Ai2-thor: An interactive 3d environment for visual ai. *arXiv preprint arXiv:1712.05474*, 2017. 3
- [26] Athanasios Krontiris, Rahul Shome, Andrew Dobson, Andrew Kimmel, and Kostas Bekris. Rearranging similar objects with a manipulator using pebble graphs. In *2014 IEEE-RAS International Conference on Humanoid Robots*, pages 1081–1087. IEEE, 2014. 2
- [27] Yann Labbé, Sergey Zagoruyko, Igor Kalevatykh, Ivan Laptev, Justin Carpentier, Mathieu Aubry, and Josef Sivic. Monte-carlo tree search for efficient visually guided rearrangement planning. *IEEE Robotics and Automation Letters*, 5(2):3715–3722, 2020. 2
- [28] Chengshu Li, Fei Xia, Roberto Martín-Martín, Michael Lingelbach, Sanjana Srivastava, Bokui Shen, Kent Vainio, Cem Gokmen, Gokul Dharan, Tanish Jain, et al. igibson 2.0: Object-centric simulation for robot learning of everyday household tasks. *arXiv preprint arXiv:2108.03272*, 2021. 3
- [29] Manyi Li, Akshay Gadi Patil, Kai Xu, Siddhartha Chaudhuri, Owais Khan, Ariel Shamir, Changhe Tu, Baoquan Chen, Daniel Cohen-Or, and Hao Zhang. Grains: Generative recursive autoencoders for indoor scenes. *ACM Transactions on Graphics (TOG)*, 38(2):1–16, 2019. 2
- [30] Qi Li, Kaichun Mo, Yanchao Yang, Hang Zhao, and Leonidas Guibas. Ifr-explore: Learning inter-object functional relationships in 3d indoor scenes. *arXiv preprint arXiv:2112.05298*, 2021. 2
- [31] Rosanne Liu, Joel Lehman, Piero Molino, Felipe Petroski Such, Eric Frank, Alex Sergeev, and Jason Yosinski. An intriguing failing of convolutional neural networks and the coordconv solution. *Advances in neural information processing systems*, 31, 2018. 15
- [32] Weiyu Liu, Chris Paxton, Tucker Hermans, and Dieter Fox. Structformer: Learning spatial structure for language-guided semantic rearrangement of novel objects. In *2022 International Conference on Robotics and Automation (ICRA)*, pages 6322–6329. IEEE, 2022. 2, 3
- [33] Andreas Lugmayr, Martin Danelljan, Andres Romero, Fisher Yu, Radu Timofte, and Luc Van Gool. Repaint: Inpainting using denoising diffusion probabilistic models. In *Proceedings of the IEEE/CVF Conference on Computer Vision and Pattern Recognition*, pages 11461–11471, 2022. 3
- [34] Andrew Luo, Zhoutong Zhang, Jiajun Wu, and Joshua B Tenenbaum. End-to-end optimization of scene layout. In *Proceedings of the IEEE/CVF Conference on Computer Vision and Pattern Recognition*, pages 3754–3763, 2020. 2
- [35] Chenlin Meng, Yang Song, Jiaming Song, Jiajun Wu, Jun-Yan Zhu, and Stefano Ermon. Sdedit: Image synthesis and editing with stochastic differential equations. *arXiv preprint arXiv:2108.01073*, 2021. 3, 8
- [36] Paul Merrell, Eric Schkufza, Zeyang Li, Maneesh Agrawala, and Vladlen Koltun. Interactive furniture layout using interior design guidelines. *ACM transactions on graphics (TOG)*, 30(4):1–10, 2011. 2
- [37] Alex Nichol, Prafulla Dhariwal, Aditya Ramesh, Pranav Shyam, Pamela Mishkin, Bob McGrew, Ilya Sutskever, and Mark Chen. Glide: Towards photorealistic image generation and editing with text-guided diffusion models. *arXiv preprint arXiv:2112.10741*, 2021. 3
- [38] Wamiq Para, Paul Guerrero, Tom Kelly, Leonidas J Guibas, and Peter Wonka. Generative layout modeling using constraint graphs. In *Proceedings of the IEEE/CVF International Conference on Computer Vision*, pages 6690–6700, 2021. 2
- [39] Despoina Paschalidou, Amlan Kar, Maria Shugrina, Karsten Kreis, Andreas Geiger, and Sanja Fidler. Atiss: Autoregressive transformers for indoor scene synthesis. In *Advances in Neural Information Processing Systems (NeurIPS)*, 2021. 2, 6, 7, 8, 14, 15
- [40] Pulak Purkait, Christopher Zach, and Ian Reid. Sg-vae: Scene grammar variational autoencoder to generate new indoor scenes. In *European Conference on Computer Vision*, pages 155–171. Springer, 2020. 2
- [41] Charles R Qi, Hao Su, Kaichun Mo, and Leonidas J Guibas. Pointnet: Deep learning on point sets for 3d classification and segmentation. In *Proceedings of the IEEE conference on computer vision and pattern recognition*, pages 652–660, 2017. 5, 12, 15
- [42] Siyuan Qi, Yixin Zhu, Siyuan Huang, Chenfanfu Jiang, and Song-Chun Zhu. Human-centric indoor scene synthesis using stochastic grammar. In *Proceedings of the IEEE Conference on Computer Vision and Pattern Recognition*, pages 5899–5908, 2018. 2
- [43] Alec Radford, Jong Wook Kim, Chris Hallacy, Aditya Ramesh, Gabriel Goh, Sandhini Agarwal, Girish Sastry, Amanda Askell, Pamela Mishkin, Jack Clark, et al. Learning transferable visual models from natural language supervision. In *International Conference on Machine Learning*, pages 8748–8763. PMLR, 2021. 3
- [44] Daniel Ritchie, Kai Wang, and Yu-an Lin. Fast and flexible indoor scene synthesis via deep convolutional generative models. In *Proceedings of the IEEE/CVF Conference on Computer Vision and Pattern Recognition*, pages 6182–6190, 2019. 2, 7
- [45] Robin Rombach, Andreas Blattmann, Dominik Lorenz, Patrick Esser, and Björn Ommer. High-resolution image synthesis with latent diffusion models. In *Proceedings of the IEEE/CVF Conference on Computer Vision and Pattern Recognition*, pages 10684–10695, 2022. 3
- [46] Yossi Rubner, Carlo Tomasi, and Leonidas J Guibas. The earth mover’s distance as a metric for image retrieval. *International journal of computer vision*, 40(2):99–121, 2000. 4
- [47] Stuart J Russell. *Artificial intelligence a modern approach*. Pearson Education, Inc., 2010. 2

- [48] Chitwan Saharia, William Chan, Huiwen Chang, Chris Lee, Jonathan Ho, Tim Salimans, David Fleet, and Mohammad Norouzi. Palette: Image-to-image diffusion models. In *ACM SIGGRAPH 2022 Conference Proceedings*, pages 1–10, 2022. 3
- [49] Rahul Sajjani, Adrien Poulenard, Jivitesh Jain, Radhika Dua, Leonidas J Guibas, and Srinath Sridhar. Condor: Self-supervised canonicalization of 3d pose for partial shapes. In *Proceedings of the IEEE/CVF Conference on Computer Vision and Pattern Recognition*, pages 16969–16979, 2022. 3, 5, 12
- [50] Jonathan Scholz and Mike Stilman. Combining motion planning and optimization for flexible robot manipulation. In *2010 10th IEEE-RAS International Conference on Humanoid Robots*, pages 80–85. IEEE, 2010. 2
- [51] Rahul Shome and Kostas E Bekris. Synchronized multi-arm rearrangement guided by mode graphs with capacity constraints. In *International Workshop on the Algorithmic Foundations of Robotics*, pages 243–260. Springer, 2020. 2
- [52] Mohit Shridhar, Lucas Manuelli, and Dieter Fox. Cliport: What and where pathways for robotic manipulation. In *Conference on Robot Learning*, pages 894–906. PMLR, 2022. 2, 3
- [53] Herbert A Simon and Allen Newell. Computer simulation of human thinking and problem solving. *Monographs of the Society for Research in Child Development*, pages 137–150, 1962. 2
- [54] Yang Song and Stefano Ermon. Generative modeling by estimating gradients of the data distribution. *Advances in Neural Information Processing Systems*, 32, 2019. 2, 3, 4
- [55] Yang Song, Jascha Sohl-Dickstein, Diederik P Kingma, Abhishek Kumar, Stefano Ermon, and Ben Poole. Score-based generative modeling through stochastic differential equations. *arXiv preprint arXiv:2011.13456*, 2020. 2, 3
- [56] Andrew Szot, Alexander Clegg, Eric Undersander, Erik Wijmans, Yili Zhao, John Turner, Noah Maestre, Mustafa Mukadam, Devendra Singh Chiplot, Oleksandr Maksymets, et al. Habitat 2.0: Training home assistants to rearrange their habitat. *Advances in Neural Information Processing Systems*, 34:251–266, 2021. 3
- [57] Jerry O Talton, Yu Lou, Steve Lesser, Jared Duke, Radomír Měch, and Vladlen Koltun. Metropolis procedural modeling. *ACM Transactions on Graphics (TOG)*, 30(2):1–14, 2011. 2
- [58] Ashish Vaswani, Noam Shazeer, Niki Parmar, Jakob Uszkoreit, Llion Jones, Aidan N Gomez, Łukasz Kaiser, and Illia Polosukhin. Attention is all you need. *Advances in neural information processing systems*, 30, 2017. 2, 3, 4
- [59] Pascal Vincent. A connection between score matching and denoising autoencoders. *Neural computation*, 23(7):1661–1674, 2011. 4
- [60] Pascal Vincent, Hugo Larochelle, Yoshua Bengio, and Pierre-Antoine Manzagol. Extracting and composing robust features with denoising autoencoders. In *Proceedings of the 25th international conference on Machine learning*, pages 1096–1103, 2008. 4
- [61] Hanqing Wang, Wei Liang, and Lap-Fai Yu. Scene mover: Automatic move planning for scene arrangement by deep reinforcement learning. *ACM Transactions on Graphics*, 39(6), 2020. 3
- [62] Kai Wang, Yu-An Lin, Ben Weissmann, Manolis Savva, Angel X Chang, and Daniel Ritchie. Planit: Planning and instantiating indoor scenes with relation graph and spatial prior networks. *ACM Transactions on Graphics (TOG)*, 38(4):1–15, 2019. 2, 7
- [63] Kai Wang, Manolis Savva, Angel X Chang, and Daniel Ritchie. Deep convolutional priors for indoor scene synthesis. *ACM Transactions on Graphics (TOG)*, 37(4):1–14, 2018. 7
- [64] Weiyue Wang, Ronald Yu, Qiangui Huang, and Ulrich Neumann. Sgpn: Similarity group proposal network for 3d point cloud instance segmentation. In *Proceedings of the IEEE conference on computer vision and pattern recognition*, pages 2569–2578, 2018. 3
- [65] Xinpeng Wang, Chandan Yeshwanth, and Matthias Nießner. Sceneformer: Indoor scene generation with transformers. In *2021 International Conference on 3D Vision (3DV)*, pages 106–115. IEEE, 2021. 2, 7
- [66] Luca Weihs, Matt Deitke, Aniruddha Kembhavi, and Roozbeh Mottaghi. Visual room rearrangement. In *Proceedings of the IEEE/CVF conference on computer vision and pattern recognition*, pages 5922–5931, 2021. 3
- [67] Tomer Weiss, Alan Litteneker, Noah Duncan, Masaki Nakada, Chenfanfu Jiang, Lap-Fai Yu, and Demetri Terzopoulos. Fast and scalable position-based layout synthesis. *IEEE Transactions on Visualization and Computer Graphics*, 25(12):3231–3243, 2018. 2
- [68] Ken Xu, James Stewart, and Eugene Fiume. Constraint-based automatic placement for scene composition. In *Graphics Interface*, volume 2, pages 25–34, 2002. 2
- [69] Yi-Ting Yeh, Lingfeng Yang, Matthew Watson, Noah D Goodman, and Pat Hanrahan. Synthesizing open worlds with constraints using locally annealed reversible jump mcmc. *ACM Transactions on Graphics (TOG)*, 31(4):1–11, 2012. 2
- [70] Li Yi, Wang Zhao, He Wang, Minhyuk Sung, and Leonidas J Guibas. Gspn: Generative shape proposal network for 3d instance segmentation in point cloud. In *Proceedings of the IEEE/CVF Conference on Computer Vision and Pattern Recognition*, pages 3947–3956, 2019. 3
- [71] Lap Fai Yu, Sai Kit Yeung, Chi Keung Tang, Demetri Terzopoulos, Tony F Chan, and Stanley J Osher. Make it home: automatic optimization of furniture arrangement. *ACM Transactions on Graphics (TOG)-Proceedings of ACM SIGGRAPH 2011*, v. 30,(4), July 2011, article no. 86, 30(4), 2011. 2
- [72] Richard Zhang, Phillip Isola, and Alexei A Efros. Colorful image colorization. In *European conference on computer vision*, pages 649–666. Springer, 2016. 4
- [73] Song-Hai Zhang, Shao-Kui Zhang, Wei-Yu Xie, Cheng-Yang Luo, and Hong-Bo Fu. Fast 3d indoor scene synthesis with discrete and exact layout pattern extraction. *arXiv preprint arXiv:2002.00328*, 2020. 2
- [74] Zaiwei Zhang, Zhenpei Yang, Chongyang Ma, Linjie Luo, Alexander Huth, Etienne Vouga, and Qixing Huang. Deep

generative modeling for scene synthesis via hybrid representations. *ACM Transactions on Graphics (TOG)*, 39(2):1–21, 2020. 2

- [75] Yi Zhou, Connelly Barnes, Jingwan Lu, Jimei Yang, and Hao Li. On the continuity of rotation representations in neural networks. In *Proceedings of the IEEE/CVF Conference on Computer Vision and Pattern Recognition*, pages 5745–5753, 2019. 3
- [76] Yang Zhou, Zachary White, and Evangelos Kalogerakis. Scenegrphnet: Neural message passing for 3d indoor scene augmentation. In *Proceedings of the IEEE/CVF International Conference on Computer Vision*, pages 7384–7392, 2019. 2

## Supplementary Document

### A. Overview

This supplementary document contains extended technical details, along with the qualitative and quantitative results that supplement the main document. After introducing our video results, we cover details of our network architectures and their applications (Sec C). We then provide detailed explanations of our two main experiment setups: Table-Chair (Sec. D), and 3D-Front (Sec. E). Next, we conduct additional analysis experiments in Sec. F. Finally, we discuss failure modes (Sec. G) and future directions (Sec. H).

### B. Video Results

In order to better visualize the 3D structures of the outputs and the denoising process, we provide videos of these processes in the format of an HTML website. We highly encourage the viewers to open the “LEGO.html” and watch the videos to fully appreciate the denoising process.

### C. Architecture Details

#### C.1. Input Object Attribute Encoding

For each object attributes  $o_i = (c_i, t_i, r_i, b_i, h_i)$ , we process it into an object token  $\delta_i \in \mathbb{R}^{512}$  to input into the transformer. The details are as follows.

We embed the translation  $t_i$ , rotation  $r_i = [\cos(\theta_i), \sin(\theta_i)]^T$ , and bounding box dimension  $b_i$  with a sinusoidal positional encoding of 32 frequencies. The frequencies are a geometric sequence with initial term 1 and common ratio  $128^{\frac{1}{31}}$ , which gives an ending term of 128. The positional encoding is therefore  $PE(x) = \{\sin(128^{\frac{j}{31}}x), \cos(128^{\frac{j}{31}}x) | 0 \leq j \leq 31\} \in \mathbb{R}^{64}$ . Applying  $PE$  to  $t_i = [t_{i,x}, t_{i,y}]$  and  $b_i = [b_{i,x}, b_{i,y}]$  gives 128-dimensional embedding, whereas applying it to  $\theta_i$  gives a 64-dimensional embedding. We then additionally process  $PE(\theta_i)$  with a linear layer mapping to  $\mathbb{R}^{128}$ .

As mentioned, for object class  $c_i$ , we utilize a 2-layer MLP with leaky ReLU activation to process the one-hot en-

coding into a 128-dimensional attribute. The above four features are concatenated to form a 512-dimensional vector.

We also optionally process a pose-invariant shape feature  $h_i$  from ConDor [49]. More specifically, we pretrained ConDor on the 3D point clouds provided by 3D-FRONT [17], and extract the product of the Tensor Field Network layer output and spherical harmonics coefficients from ConDor to provide pose-invariant features capturing the shape of each object  $\mathbb{R}^{1024 \times 128}$ . Taking the mean across the 1024 points gives a 128-dimensional feature, which we then pass through a 2-layer MLP with leaky ReLU activation to obtain the final shape feature  $\in \mathbb{R}^{128}$ . We apply the shape feature  $h_i$  on the *Grouping by Shape* to demonstrate its effectiveness.

Finally, the concatenated object attributes  $o'_i = (c'_i, t'_i, r'_i, b'_i, h'_i) \in \mathbb{R}^{640}$  are processed through 2 linear layers with leaky ReLU activation to produce a 512-dimensional object token for the transformer. Note that if floor plan is utilized, we modify the final layer to produce a 511-dimensional feature, and utilize the last bit to distinguish object tokens from floor plan tokens.

#### C.2. Floor Plan Encoder Architecture

We represent each floor plan as 250 randomly sampled contour points. We represent each point with its 2D position coordinate and the 2D normal of the line it is on. In aggregate, we represent each floor plan with a feature in  $\mathbb{R}^{250 \times 4}$ .

We employ a simplified PointNet [41] as the floor plan encoder to extract one unified floor plan feature from this representation. The encoder first processes the feature with 3 linear layers and Leaky ReLU activation, mapping the feature dimension through [4, 64, 64, 512]. Then, we max pool the resulting embedding in  $\mathbb{R}^{250 \times 512}$  to obtain a global floor-plan encoding in  $\mathbb{R}^{512}$ . We then pass this global representation through one final linear layer and append a binary bit distinguishing it from object tokens. Finally, we combine this floor plan token with the  $|\tilde{X}|$  number of 512-dimensional object tokens and pass the resulting  $(|\tilde{X}| + 1) \times 512$  input matrix to the transformer.

#### C.3. Output Layers

The transformer outputs  $(|\tilde{X}| + 1) \times 512$  feature tokens. We ignore the background floor plan token and use the  $|\tilde{X}|$  object tokens to predict clean transformations. We apply 2 linear layers with leaky ReLU activation to the output tokens to map to 256 dimensions then 4 dimensions and obtain the final absolute transformation predictions.

#### C.4. Inference Langevin Dynamics Parameters

During inference, we use the Langevin Dynamics scheme to iteratively denoise a messy scene input. As mentioned, for time step  $\tau$ , we select  $\alpha(\tau) = \alpha_0 / (1 + a_1 * \tau)$



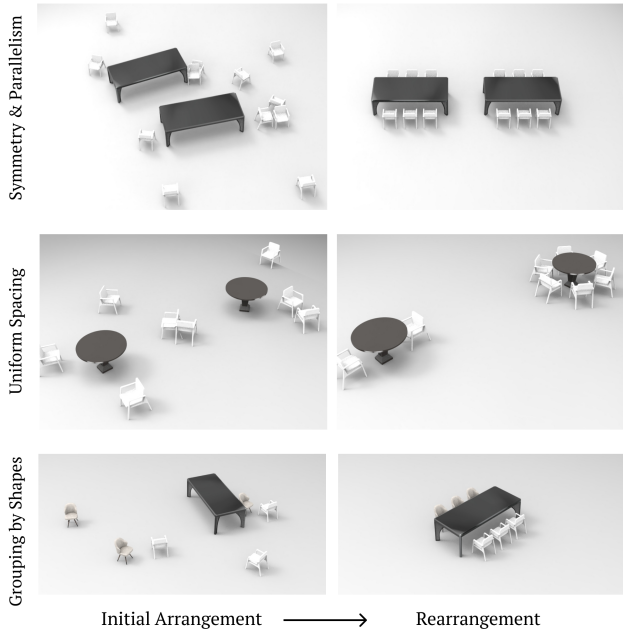


Figure 9. Regularities learning results (additional visualizations). We train our denoising network to learn three different regularities. LEGO-Net learns the complex regularity rules as demonstrated by the iterative denoising results shown on the right. Zoom in for details, especially for the shape-based grouping.

to regulate the step size and  $\beta(\tau) = \beta_0 * b_1^{\lfloor \tau/b_2 \rfloor}$  to regulate the noise added at each iteration. We empirically select  $a_1 = 0.005$  and  $b_1 = 0.9$ . For the living room, we adopt  $\alpha_0 = 0.1$ ,  $\beta_0 = 0.01$ , and  $b_2 = 10$ . For bedroom, we adopt  $\alpha_0 = 0.08$ ,  $\beta_0 = 0.008$ , and  $b_2 = 8$ .

We break from the iterative denoising process upon any one of two conditions: (1) if for 3 consecutive iterations, both the predicted translation displacement vector has Frobenius norm less than 0.01 and the predicted rotation angle displacement is less than 0.005 radians, or (2) we have reached 1500 iterations.

## D. Table-Chair Experiment

### D.1. Data Generation

To analyze the regularities our model can capture, we proposed 3 synthetic Table-Chair experiment settings, with a focus on Symmetry and Parallelism, Uniform Spacing, and Grouping by Shape respectively.

For each of the proposed experiments, we generate clean scenes based on designed rules and take a bimodal approach at perturbations when generating clean-messy training data pair. More specifically, for half of the synthesized clean scenes, we employ a Gaussian noise kernel whose standard deviation is drawn from a Gaussian distribution with a small standard deviation (0.01 for translation and  $\pi/90$  for rota-

tion angle). For the other half of the clean scenes, we employ a Gaussian noise kernel whose standard deviation is drawn from a Gaussian distribution with a relatively larger standard deviation (0.25 for translation and  $\pi/4$  for rotation angle). We follow the same paradigm as the 3D-FRONT experiments for the rest of the training details.

### D.2. Inference Parameters

As for the 3D-FRONT experiments, we employ the Langevin Dynamics scheme to rearrange a given perturbed Table-Chair arrangement. We empirically adjust the parameters to slightly increase the step size, accelerate the noise decay schedule, and loosen the termination condition. In particular, we select  $\alpha_0 = 0.12$ ,  $a_1 = 0.005$ ,  $\beta_0 = 0.01$ ,  $b_1 = 0.9$ ,  $b_2 = 2$ , and terminate once the prediction displacements are small enough in magnitude for 1 iteration.

### D.3. Success Rate

As mentioned, we measure LEGO-Net’s performance in each Table-Chair environment through the success rate of its rearrangement, whose criteria we will now elaborate on.

**Symmetry and Parallelism:** For a rearrangement to be classified as a success, it must satisfy the following conditions:

- The mean euclidean distance of per-object movement averaged across scenes is less than 0.5.
- For each chair, the angular offset between its orientation and the table-facing orientation (top-row chairs face negative y-axis; bottom-row chairs face positive y-axis) is less than  $\pi/60$  radians.
- Given the two final rearranged table positions, we compute their respective chair positions and perform Earth Mover’s Distance assignment from the final predicted chair positions to them. The total distances summed across all 12 chairs for the 2 tables need to be less than 0.08. Note that this metric integrates collinearity, parallelism, and symmetry, and penalizes collision.

**Uniform Spacing:** For a rearrangement in the Uniform Spacing experiment to be classified as a success, it must satisfy the first two criteria for the Symmetry and Parallelism experiment. Namely, the mean per-object movement needs to be less than 0.5 and the angular offset between each chair’s denoised orientation and the table-facing orientation needs to be less than  $\pi/60$  radians.

Because the number of chairs arranged around each of the 2 circular tables is variable, we cannot formulate the Earth Mover’s Distance assignment as in the Symmetry and Parallelism experiment. Instead, to measure how well an arrangement captures the object-object relationships and regular relative positioning, we compute two other metrics. For

each table, we compute the angular distances between each adjacent pair of its chairs and measure the variance of these distances. We designate that a successful arrangement must have an angular distance variance of less than 0.009 radians.

Additionally, given we utilize a fixed radius to generate clean chair arrangements around a table, we can measure the mean difference between the chair-to-closest-table distance and this radius, and we designate that the absolute difference needs to be less than 0.01 for an arrangement to be considered successful.

**Grouping by Shape:** Similarly, for a rearrangement in the Grouping by Shape experiment to be classified as a success, it must satisfy the first two criteria for the Symmetry and Parallelism experiment: the mean per-object movement needs to be less than 0.5 and the angular offset for each chair’s orientation needs to be less than  $\pi/60$  radians. Additionally, we once again can compute the exact regular arrangement of chairs with respect to the table, enabling us to calculate the Earth Mover’s Distance from the final predicted chair positions to the clean configuration with respect to the predicted table position. We designate that the distance summed across the 6 chairs needs to be less than 0.05.

Furthermore, to measure success at grouping, we designate that each row must be assigned exactly 3 chairs and that all chairs assigned to the same row must have the same shape feature.

#### D.4. Additional Qualitative Results

In Fig. 9, we provide additional qualitative renderings for the three Table-Chair experiments.

### E. 3D-FRONT Experiment

To process the 3D-FRONT dataset [17], we closely follow the preprocessing protocol of ATISS [39]. For each scene, we extract from the given meshes and parameters the translation, rotation, class, and bounding box size for every object, and we normalize all lengths to be in  $[-1, 1]$ . We additionally extract accurate contours of the floor plans by running an iterative closest point algorithm [3] using the contour corner points of ATISS’s binary floor plan masks as the source and the relevant vertices from 3D-FRONT floor mesh as the target.

#### E.1. Baseline Description

We compare against three variants of ATISS: *vanilla*, *labels*, and *failure-correction*. As described in the main text, *vanilla* is the original ATISS approach that generates a scene from scratch given the floor plan. ATISS *labels* is given a set of furniture labels and a floor plan and samples of the transformations and sizes for the labeled objects. ATISS *failure-correction* is proposed as an application to

the probabilistic generative modeling of ATISS. It identifies which object is likely to be a failure and resamples that object given all the other objects. While the original paper only showed the technique to work when a single object is perturbed, we find it reasonable to extend the algorithm to multi-object perturbation cases. Specifically, we provide a scene with all objects perturbed (same input as LEGO-Net) and iteratively resample the lowest-probable object. We stop the iteration when it reaches 1,000 times or the minimum probability is higher than a manually set threshold. We note that while *failure-correction* did not perform as expected when all of the objects are perturbed, as shown in Fig. 10, it is the closest baseline we could find in the literature that performs data-driven denoising of a scene. For the comparison, we use the official training and testing code provided by the authors of ATISS without modifications. For ATISS *failure-correction*, we add a for-loop and stopping criteria on top of their implementation, and set the scales of objects back to the original input to follow our use case.

#### E.2. Metric Description

For FID and KID computation, we first generate the same number of scenes as in the test dataset. Then we randomly select 500 scenes from them and have another 500 randomly selected real scenes from the 3DFRONT dataset. For both FID and KID, we repeat the metric computation 5 times and report the average. Note that for computing the FID score for ATISS, we used the officially provided code to follow their exact evaluation procedure, but we failed to reproduce their numbers. Hence, we use our own way of computing the metrics and report only ours.

We note that the Frechet Inception Distance (FID) [18] is known to present significant positive bias when the number of images is small (e.g.,  $\leq 2000$ ). In our case, we’re dealing with an even smaller number of test images (a few hundred). Therefore, to compute a metric that is less biased in the small-data regime, we adopt the Kernel Inception Distance [4], which is known to address the bias problem and presents small variance even at a few hundred samples.

**Distance Traveled.** As discussed in the main text, we aim at rearranging the messy scenes while retaining the flavor of the original scenes. Practically, cleaning a room should move objects as small as possible while applying regularities. Therefore, we measure and report the mean of the average distance traveled for scenes.

This distance traveled metric for each scene is measured by computing the average Euclidean distance between the corresponding objects between the initial and final states. Note that for the vanilla ATISS, this metric is not applicable, because the method randomly puts objects into the scene, hence the correspondences cannot be obtained. However, for ATISS *failure-correction*, we compute this metric

	Bedroom $\uparrow$	Living Room $\uparrow$
PointNet W/O Noise	<b>84.4%</b>	<b>54.4%</b>
PointNet W/ Noise	84.2%	54.2%
ResNet W/O Noise	83.8%	54%
ResNet W/ Noise	83.6%	54.2%

Table 3. Percentage of denoised scenes with 90% of its furniture within the boundaries of the floor plans. We train and test our method using different floor plan encoding architectures (PointNet vs ResNet), and measure the percentage of the denoised scenes where all furniture respect the floor boundaries.

by computing the difference between the initial position of each object and their final locations after the correcting algorithm is applied.

**EMD to GT.** In order to measure how accurately our method recovers the original scene configuration, we introduce the metric to measure the distance (in Earth Mover’s Distance) between the final and the ground truth scene states. Note that computing the difference between the denoising prediction and the ground truth is widely used in the image-denoising literature, using such metrics as PSNR or SSIM [20]. ATISS *vanilla* and *labels* do not receive the messy scene as input, so this metric is not applicable to them. However, ATISS *failure-correction* directly fixes the input scene, thus we measure how accurately they recover the original clean scene. Finally, we note that the EMD to GT metric becomes highly noisy and irrelevant when the noise added to perturb the clean scene becomes too high when there is barely any locational information left in the messy inputs.

### E.3. Additional Qualitative Results

We provide additional qualitative results on the 3D-Front dataset, comparing against the closest method on the scene rearrangement task, ATISS *failure-correction* in Fig. 10. We additionally show the qualitative results of our method on 3D-Front dataset in Fig. 16.

## F. Analysis (Continued)

### F.1. Enforcing Floor Plan Constraints

In this section, we analyze our choice of floor plan encoder. As described in the main paper, we extract point clouds on the boundary of the binary floor plan mask, and process them with a PointNet [41] to obtain a single feature vector. We note that, in ATISS [39], a 2D convolutional network with residual connections (ResNet) was used to process the floor plans. Here, we conduct an experiment to justify our use of PointNet architecture. As a baseline, we use a ResNet architecture from ATISS, but augment the input floor plan to add two channels corresponding to the  $xy$

coordinate for each pixel center, which is known to provide “spatial awareness” to the 2D CNN (in CoordConv [31]). We expect this variant of ResNet should work at least as well as the vanilla ResNet with binary mask input used in ATISS.

To compare the two methods of floor plan encoding, we train the two variants of the model using different floor plan encoding architectures, i.e., ResNet vs PointNet. To test the effectiveness of the two encodings, we measure how often furniture gets out of the floor boundaries. Specifically, a scene is a success when 90% of objects are within the floor boundary with 4% of its length margin. While respecting the floor boundaries does not necessarily lead to high-quality, regular scenes, we empirically find this metric as a reasonable proxy. As can be seen from the numerical results of Tab. 3, the use of PointNet outperforms that of ResNet by a slight margin, in terms of the percentage of scenes where all furniture respected the boundary. However, we note that using PointNet is significantly faster, having almost no computational overhead for operating on the sampled 250 boundary points. We, therefore, choose to use the simpler but similar-performing PointNet to encode the scene floor plans.

### F.2. Relative vs Absolute

2D diffusion models perform better at predicting the noise instead of the un-noised images [19]. However, in our setting, we observed that the relative predictions in the Table-Chair environment significantly underperform the absolute variant. This could be partly explained by the fact that there is only a limited number of rotations of objects occurring in regular scenes. For the location of objects, we have tried training the network with relative coordinates but didn’t observe any meaningful boost in performance. We believe that applying relative location learning is an important future topic for enabling larger-scale rearrangement problems.

Relative transformation predictions offer translation invariance, which is particularly valuable for large-scale scenes. However, for our setting, we observed that the absolute prediction models generally outperform their relative counterparts. We trained 3 variants of the same architecture network for the Uniform & Parallelism setting: (i) absolute translation and rotation prediction, (ii) relative translation and rotation prediction, and (iii) relative translation and absolute rotation prediction.

Following the criteria in D.3, both variants (ii) and (iii) surprisingly report the success rate of 0%. Upon further investigation, they perform comparably, if not better, at limiting the distance of movement and orienting chairs to face the tables, but they significantly underperform (i) in terms of Earth Mover’s Distance to Ground Truth chair positions with respect to the predicted table position. With the same



Figure 10. Qualitative comparison against ATISS-failure-correction. We show qualitative examples illustrating the difference in behaviors between our method and the closest competitor, ATISS *failure-correction*. Being a generative model, ATISS is able to compute the probability of the current object transformations and resample the ones with low probability. While ATISS has demonstrated great results in their paper when there is only one object being perturbed, we observe that when *all* objects are perturbed ATISS failure-correction has a hard time fixing it correctly. We hypothesize that this is due to the one-prediction-at-a-time nature of ATISS – it is difficult to find a good location to put the current object when all the other objects are perturbed. On the other hand, our method simultaneously optimizes for all the objects, avoiding such difficulty. Even for the highly challenging scene structure of the second row, our method provides high-quality layouts, while ATISS failure-correction fails to find regular rearrangement.

denoising parameters, the relative variants consistently fail to place the chairs as precisely as the absolute variant. This observed deficiency may diminish as the complexity of the scene increases.

We believe that relative transformation prediction is an important future direction to explore. Currently, our input object attribute’s transformations are global, and thus our system is not translationally invariant. An interesting direction for future investigation is to explore a sliding-window-style input processing to ensure translation invariance and to apply positional encoding to the output transformations.

### F.3. Distance to Ground Truth and Distance Moved vs. Noise

Since the task of rearrangement values affinity to the starting configuration of objects, one question of interest is how closely we recover the original clean arrangement when given a perturbed version of it, versus another possibly equally valid, clean arrangement. Its correlation with the level of noise added is intuitive—we expect that when the perturbation is low, we more closely reconstruct the original scene whereas when the perturbation is high, our model

	Distance Moved ↓	Direction Offset ↓	EMD to GT ↓
Absolute	2.98e-1	1.10e-3	<b>5.16e-2</b>
Relative	<b>2.47e-1</b>	<b>4.21e-4</b>	1.58e-1
Relative Translation & Absolute Rotation	2.73e-1	5.18e-4	2.83e-1

Table 4. Mean statistics from denoising results with the gradient with noise strategy. The relative prediction model slightly outperforms the absolute prediction model in terms of distance moved and angular orientation offset, but it performs much worse in terms of EMD to GT as although it maps objects to the right general region, it does not place them as precisely as the absolute model.

may choose a regular arrangement different from that of the original scene in an effort to minimize the distance moved (see Fig. 11). This is indeed what we have observed numerically, as shown in Fig 13.

Note that with a low degree of noise, our model performs the task of rearrangement, but as the degree of noise increases, our model gradually transitions to the task of



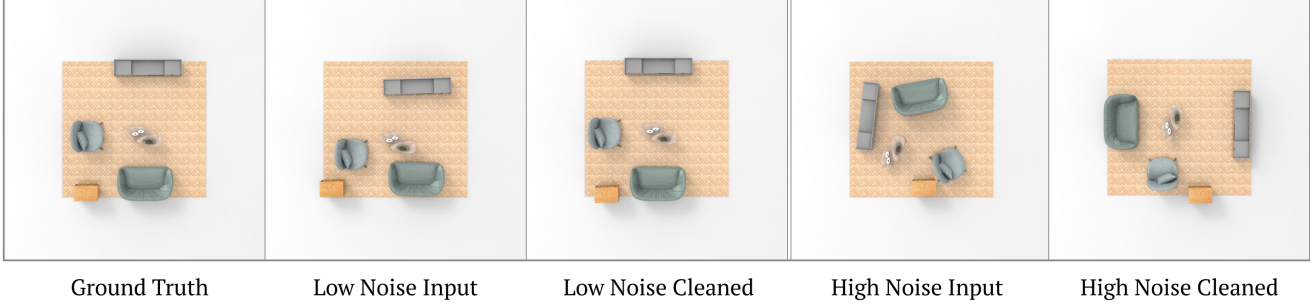


Figure 11. LEGO-Net denoising results on different noise levels (additional visualization to Fig.6 of the main document). When the perturbation added to the scene is low, LEGO-Net is able to closely reconstruct the clean version of the scene. In contrast, when the noise level is high, our denoising process finds a different realization of a regular scene, behaving more like an unconditional model. We provide numerical evidence for this phenomenon in Tab. 13.

arrangement. In the extreme case where we give LEGO-Net a scene with objects outside of the floor plan, LEGO-Net is able to perform scene arrangement from scratch (see Fig. 12).

The open-endedness in the definition of regularity is one of the reasons why this task is both challenging and interesting. The interpolation-like behavior of LEGO-Net conditioned on the degree of noise signifies the learnable relationship between rearrangement and synthesis and demonstrates that a diffusion-like approach beholds promising potential at such open tasks.

#### F.4. Integer Relations

The task of evaluating regularity in an object arrangement is itself an interesting research problem because, in general, multiple regular solutions are possible. To evaluate and quantify the notion of “regularity” in object arrangements, we propose using number-theoretic machinery for detecting and evaluating sparse linear integer relations among object coordinates. That is, given coordinates  $t_i$ ’s for  $n$  objects, we seek to find integer coefficients  $a_i$ ’s such that:

$$a_1 t_1 + \dots + a_n t_n = 0, \quad 0 < |a_i| < \eta, \forall a_i, \quad (7)$$

For simplicity, we consider each dimension of the coordinates separately, i.e.,  $t_i \in \mathbb{R}$ . Additionally, in practice, we introduce an additional parameter  $\epsilon$  to control the precision of the solutions found. In particular, we seek to find relationships such that  $|a_1 t_1 + \dots + a_n t_n| < \epsilon$ . For our evaluation, we fix  $\epsilon = 0.01$  to focus on the near-perfect relations while allowing some leeway for insignificant offsets. To efficiently find these integer solutions, we employ the PSLQ algorithm [15].

When the subset size  $n$  and maximum coefficient magnitude constraint  $\eta$  are small, the integer relations can be intuitively understood (e.g. representing co-linearity, symmetry, uniform spacing among few objects). To capture

more complex and more general notion of regularity, we increase  $n$  and  $\eta$ . Doing so precipitates two challenges. First, the number of possible subsets of size  $n$  for each scene increases rapidly as  $n$  increases, compromising efficiency. Secondly, experimentally running the algorithm on pure noise shows that with looser constraints, we may find many trivial relations that do not appear to correspond to high-level ‘cleanness’. To counter these, we introduce two filtering mechanisms to increase the subset sampling efficiency and to filter out the insignificant relations.

We observe that regularities of interest to us mostly occur among objects in close proximity to one another, such as tables and chairs. Therefore, for  $n > 2$ , instead of sampling from all possible subsets of the objects in the scene, we iterate through each object and sample from the object’s positional neighborhood. For  $n = 3$ , for each object, we sample 2 from the closest 4 neighboring objects to form  $\{t_1, t_2, t_3\}$ . This greatly improves sampling efficiency, and it also helps eliminate irrelevant candidates as integer relations satisfied by objects in vicinity to one another are more likely to be meaningful for the purpose of our evaluations.

Additionally, to filter out relations that may have been satisfied by numerical coincidence, we require all relations to be translation-invariant. Specifically, for each subset, we sample a noise  $\mu$  from uniform distribution  $U(-1, 1)$  and apply the algorithm to  $\{t_1 + \mu, \dots, t_n + \mu\}$ . We repeat the process 10 times and only deem a subset to have a valid relation if the algorithm succeeds for all 10 times. This helps the metric to focus on regularities with respect to the relative positions instead of the absolute positions of objects.

In Fig 14, we demonstrate that with these two filtering mechanisms, our metric is still meaningful for  $\eta = 5$  and potentially larger parameters, which would be useful for measuring wider ranges of regularities. We also show that averaging all the integer relation chances across our experiments in Fig. 6 and Fig. 14 to suggest more general notions of regularity, using which LEGO-Net outperforms the ATISS variants.

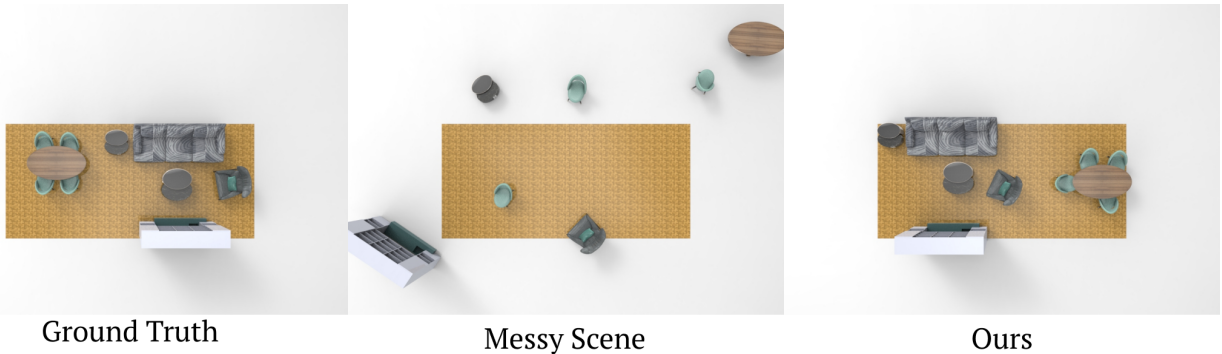


Figure 12. Extreme case rearrangement. When we add an extraordinarily high amount of noise to the scene, the original structure of the scene is gone. In this case, running our denoising algorithm amounts to running an unconditional sampling, leading to a scene arrangement significantly different from the ground truth.

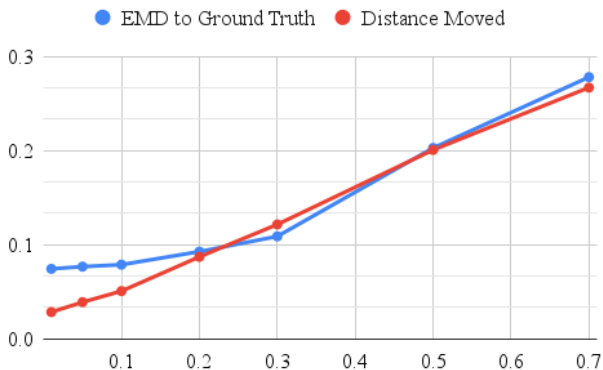


Figure 13. LEGO-Net denoising results on different noise levels (supplementing Fig. 7 of the main document). The horizontal axis specifies the standard deviation of the gaussian distribution from which the (translation) noise level is drawn, and the vertical axis specifies the distance in the normalized scene of range  $[-1, 1]$ . We computed mean statistics across 100 scenes at translation noise level standard deviations  $[0.01, 0.05, 0.1, 0.2, 0.3, 0.5, 0.7]$  and rotation angle noise level standard deviation  $[\pi/90, \pi/24, \pi/12, \pi/4, \pi/3, \pi/2, \pi]$ . When the perturbation added to the scene is low, LEGO-Net is able to closely reconstruct the clean version of the scene while minimizing the distance moved. In contrast, when the noise level is high, our denoising process may find a different realization of a regular scene to maintain a low distance moved, behaving more like an unconditional model.

### G. Failure Modes

While LEGO-Net generates unprecedented-quality indoor scenes through the iterative denoising process, we notice that it often suffers from objects going out of the floor boundaries and objects penetrating each other. These failure modes are illustrated in Fig. 15. In fact, we measure that in Tab 3 that around half of living realizations have at least one object outside of the boundaries.

We propose two possible remedies for these related issues. First, we could apply post-processing steps to physically resolve the two issues. That is, we optimize the locations of the objects within the scene such that penetrations and out-of-boundary issues are resolved and at the same time minimize the required movement. We believe a possible formulation would involve a signed distance function (SDF), where you can easily compute the gradient to minimize the penetrations. That is, when a point lies on the negative territory of another shape’s SDF, we can optimize the location of that point out towards the SDF’s gradient directions.

Secondly, one can consider encoding the floor plan to obtain a richer set of features. One possibility is to encode each line segment of the floor plan separately as a token. This will essentially treat each line segment as an object in the scene and could enforce stricter constraints on the boundaries. At a glance, this strategy might increase the computational cost significantly, due to the quadratic nature of Transformer time complexity. However, one could consider limiting the communications between the line segment tokens to prevent quadratic scaling of the complexity.

We leave these two potential remedies for our failure modes as future work.

### H. Future Work

In this work, we introduced LEGO-Net, an iterative-denoising-based method for tackling scene rearrangement task, which is relatively understudied compared to the scene synthesis task. We show through extensive experiments that our method is able to capture regularities of complex scenes, generating high-quality object rearrangements that could not be achieved by existing approaches to date.

However, LEGO-Net in its current form only operates on a 2D plane for the rearrangement. Extending our work to operate on the  $SE(3)$  transformation space would make it more applicable to real-world scenes. A significant bar-

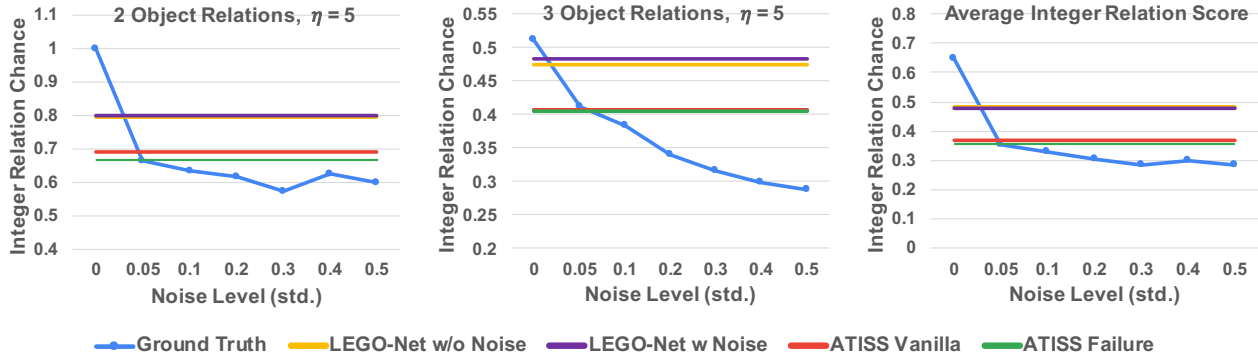


Figure 14. We measure the chance of finding integer relations among the coordinates of two (left) and three (middle) objects within a Living Room scene for  $\eta = 5$ . We additionally aggregate these two settings with the two presented in Fig 6 to produce an overall average integer relation score (right) for measuring general regularity. We normalize all raw chance measures by the maximal chance across the four settings, and the numerical values are thus all directly comparable. Note that LEGO-Net outperforms the ATISS variants for  $\eta = 5$  as well as on the average score.

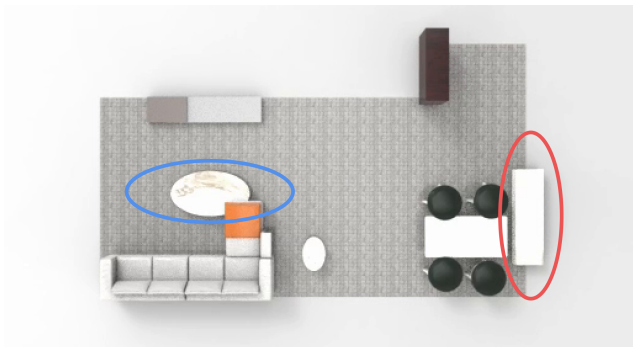


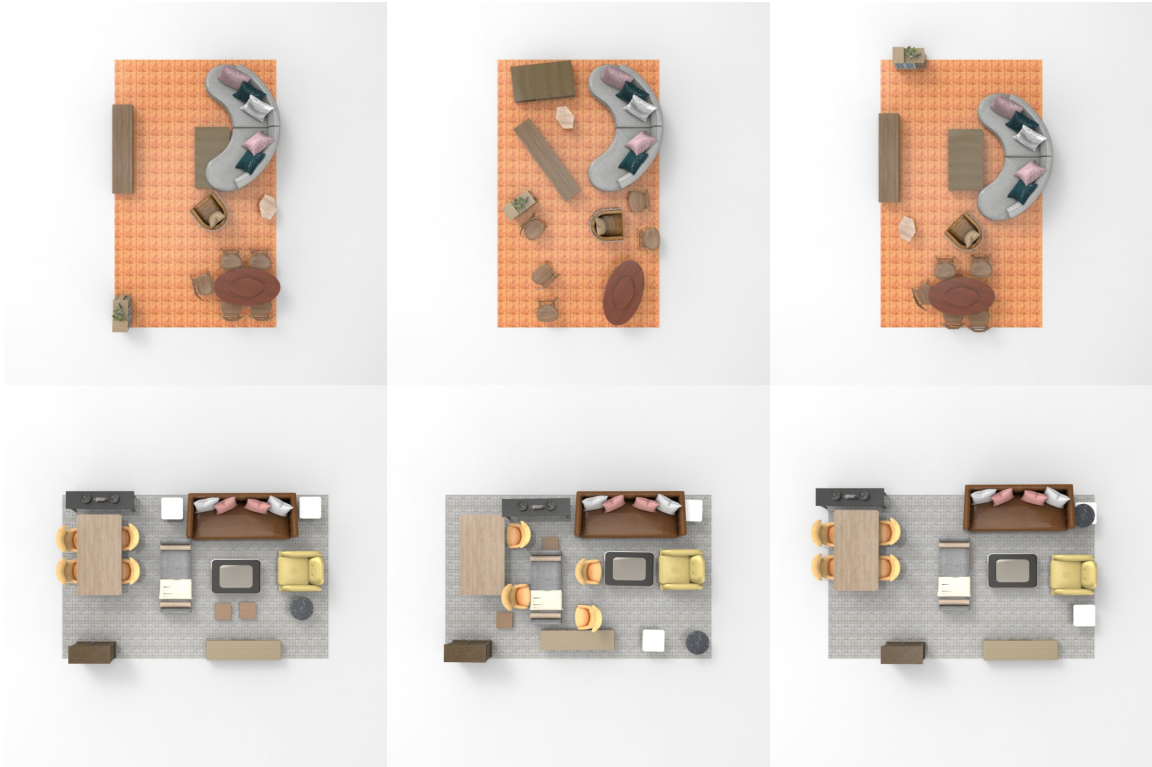
Figure 15. Failure modes. While LEGO-Net generates high-quality scenes, it often exhibits the two failure modes of placing objects outside of the floor plan boundaries (red ellipse) and inducing penetration between objects (blue ellipse). We leave post-processing steps to resolve these issues as future work.

rior to achieving 3D rearrangement is the lack of data. We notice that most of the indoor scene arrangement datasets deal with objects laid on the floor plan, which could limit the progress of studying  $SE(3)$  scene arrangements. Designing and collecting such a dataset, e.g., small objects on top of each other is an interesting future direction.

Moreover, the trajectories generated during the denoising process of LEGO-Net are not meant to respect physical constraints, e.g., penetrations and collisions. We find that enforcing the physical constraints during the denoising steps could significantly limit the space of possible scene rearrangement. Currently, when one wants to move the objects following the initial and final state of our algorithm, one needs to run a motion planning algorithm. Extending our work to output motion plans, along with the final states, is worth pursuing.

Finally, LEGO-Net has only been shown to work well on relatively small room-scale scenes. Extending our work

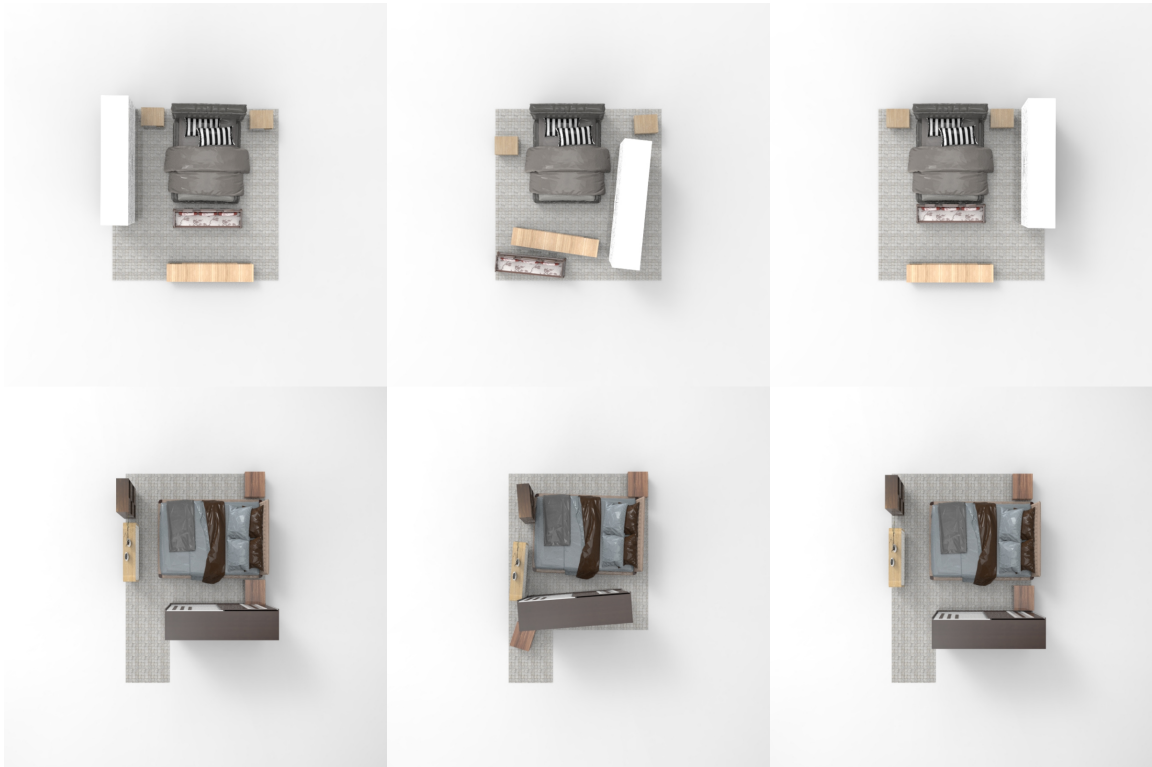
to operate on larger scale scenes, e.g., rearranging warehouses might require changes in some of our architectures, including strengthening translational invariance. Exploring such strategies remains an understudied challenge, which we continue to explore.



Ground Truth

Messy Scene

Our Rearrangement



Ground Truth

Messy Scene

Our Rearrangement

Figure 16. Additional rearrangement results on 3D-Front dataset.